IDENTIFYING ISOTROPIC EVENTS USING A REGIONAL MOMENT TENSOR INVERSION

Sean R. Ford[1,2], Douglas S. Dreger[1], and William R. Walter[2]

Berkeley Seismological Laboratory[1] and Lawrence Livermore National Laboratory[2]

Sponsored by National Nuclear Security Administration

Contract Nos. DE-FC52-06NA27324[1] and AC52-07NA27344[2]
Proposal No. BAA06-42

ABSTRACT

The deviatoric and isotropic source components for 17 explosions at the Nevada Test Site, as well as 12 earthquakes and 3 collapses in the surrounding region of the western US, are calculated using a regional time-domain full waveform inversion for the complete moment tensor. The events separate into specific populations according to their deviation from a pure double-couple and ratio of isotropic to deviatoric energy. The separation allows for anomalous event identification and discrimination between explosions, earthquakes, and collapses. Confidence regions of the model parameters are estimated from the data misfit by assuming normally distributed parameter values. We investigate the sensitivity of the resolved parameters of an explosion to imperfect Earth models, inaccurate event depths, and data with a low signal-to-noise ratio (SNR) assuming a reasonable azimuthal distribution of stations. In the band of interest (0.02–0.10 Hz) the source-type calculated from complete moment tensor inversion is insensitive to velocity model perturbations that cause less than a half-cycle shift (<5 sec) in arrival time error if shifting of the waveforms is allowed. The explosion source-type is insensitive to an incorrect depth assumption (for a true depth of 1 km), but the goodness-of-fit of the inversion result cannot be used to resolve the true depth of the explosion. Noise degrades the explosive character of the result, and a good fit and accurate result are obtained when the SNR is greater than 5. We assess the depth and frequency dependence upon the resolved explosive moment. As the depth decreases from 1 km to 200 m, the isotropic moment is no longer accurately resolved and is in error between 50% and 200%. However, even at the most shallow depth the resultant moment tensor is dominated by the explosive component when the data has a good SNR. The sensitivity investigation is extended via the introduction of the network sensitivity solution, which takes into account the unique station distribution, frequency band, and SNR of a given test scenario. An example of this analysis is presented for the North Korea test, which shows that in order to constrain the explosive component one needs a certain station configuration. In the future we will analyze the bias in the source-type parameters due to error in the Green's function by incorporating a suite of suitable velocity models in the inversion.

Report Documentation Page

Form Approved
OMB No. 0704-0188

1. REPORT DATE	2. REPORT TYPE	3. DATES COVERED
SEP 2008		**00-00-2008 to 00-00-2008**

4. TITLE AND SUBTITLE	5a. CONTRACT NUMBER
Identifying Isotropic Events Using a Regional Moment Tensor Inversion	5b. GRANT NUMBER
	5c. PROGRAM ELEMENT NUMBER
6. AUTHOR(S)	5d. PROJECT NUMBER
	5e. TASK NUMBER
	5f. WORK UNIT NUMBER
7. PERFORMING ORGANIZATION NAME(S) AND ADDRESS(ES) **Berkeley Seismological Laboratory,215 Mccone Hall ,Berkeley ,CA,94720-4760**	8. PERFORMING ORGANIZATION REPORT NUMBER
9. SPONSORING/MONITORING AGENCY NAME(S) AND ADDRESS(ES)	10. SPONSOR/MONITOR'S ACRONYM(S)
	11. SPONSOR/MONITOR'S REPORT NUMBER(S)

12. DISTRIBUTION/AVAILABILITY STATEMENT
Approved for public release; distribution unlimited

13. SUPPLEMENTARY NOTES
Proceedings of the 30th Monitoring Research Review: Ground-Based Nuclear Explosion Monitoring Technologies, 23-25 Sep 2008, Portsmouth, VA sponsored by the National Nuclear Security Administration (NNSA) and the Air Force Research Laboratory (AFRL)

14. ABSTRACT
see report

15. SUBJECT TERMS

16. SECURITY CLASSIFICATION OF:			17. LIMITATION OF ABSTRACT	18. NUMBER OF PAGES	19a. NAME OF RESPONSIBLE PERSON
a. REPORT	b. ABSTRACT	c. THIS PAGE			
unclassified	**unclassified**	**unclassified**	**Same as Report (SAR)**	**10**	

OBJECTIVES

We implement the time-domain full-waveform inversion of regional data for the complete moment tensor devised by Minson and Dreger (2008) after Herrmann and Hutcheson (1993) based on the work of Langston (1981). In general, synthetic seismograms are represented as the linear combination of fundamental Green's functions where the weights on these Green's functions are the individual moment tensor elements. The Green's functions for a one-dimensional (1-D) velocity model of eastern California and western Nevada (Song et al., 1996) are calculated as synthetic displacement seismograms using a frequency-wavenumber integration method (Saikia, 1994). The synthetic data are filtered with a 4-pole acausal Butterworth filter with a low corner of 0.02 Hz and a high corner of 0.05 Hz and 0.1 Hz for events with $M_W \geq 4$ and $M_W < 4$, respectively. At these frequencies, where dominant wavelengths are tens of kilometers, we assume a point source for the low-magnitude regional events investigated in this study. The point source assumption allows for linearization in the time-domain, which is where we carry out the least-squares inversion.

RESEARCH ACCOMPLISHED

We analyzed events that were digitally recorded with a high signal-to-noise ratio by more than two regional broadband stations. Three-component data were collected from a total of 52 stations from the US National Seismic Network, IRIS/USGS, Berkeley Digital Seismic Network, Trinet, and the Lawrence Livermore National Laboratory (LLNL) network (Figure 1). All data is freely available from IRIS via the internet except the LLNL historic network data, which is available on compact disk (Walter et al., 2004). Not all stations recorded all events, and a total of 16 stations were used in the inversion of the explosion data, which are listed in Figure 1. We remove the instrument response, rotate to the great-circle frame, integrate to obtain displacement, and use the same filter as for the synthetic seismograms. The LLNL network (white triangles in Figure 1) was composed of Sprengnether instruments with limited long-period response, and for those data we used a passband of 10–30 seconds for both the data and synthetics.

We calibrated the algorithm by calculating the full moment tensor for the 1992 Little Skull Mountain event. We find a solution at all depths within 5 km of the reported depth. The depth that produces Green's functions that best fit the data is used in the final solution. Fit is quantified by the variance reduction (VR), which is a normalized variance given by

$$\mathrm{VR} = \left[1 - \frac{\sum_i (d_i - s_i)^2}{\sum_i d_i^2} \right] \times 100 \ ,$$

where i are the displacements at all times for all components at all stations, and d and s are the data and synthetic, respectively.

We also allow the Green's functions calculated at a given distance to shift relative to the data to address small hypocentral errors and uncertainty in the velocity model used to compute the Green's functions. The shift that produces the best fit is used in the final solution. We limit the shift to less than 5 and 3 sec for high-pass corners of 0.05 and 0.10 Hz, respectively. The allowed time shift is large enough to make up for small hypocentral errors, but small enough to disallow cycle-skipping that could produce erroneous mechanisms. The sensitivity of the time shift relative to the assumed velocity model will be discussed later in the paper. The full moment tensor solution is decomposed to an isotropic and deviatoric component. We calculate the total scalar moment (M_0) as

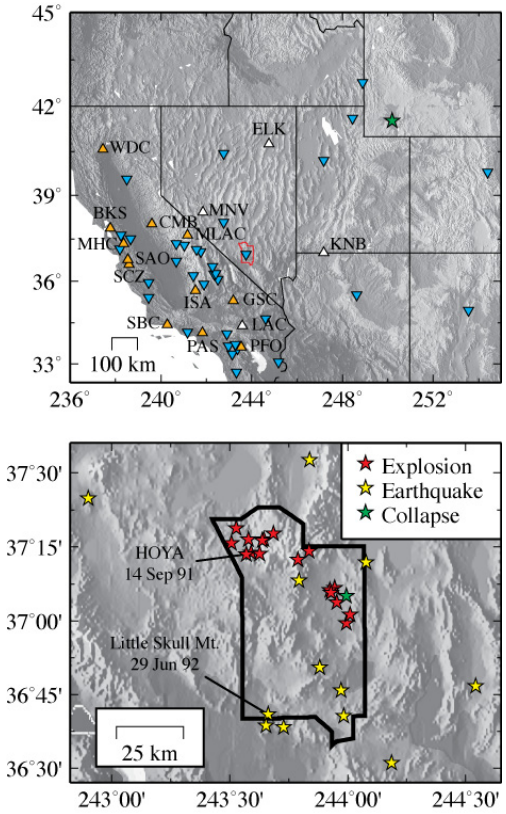

Figure 1. Map of the Western US with stations (blue inverted triangles), earthquakes (yellow stars), explosions (red stars), and collapses (green stars) used in this study. The bottom panel is a blow-up of the Nevada Test Site (NTS) region with the NTS outlined in black and in the top panel in red.

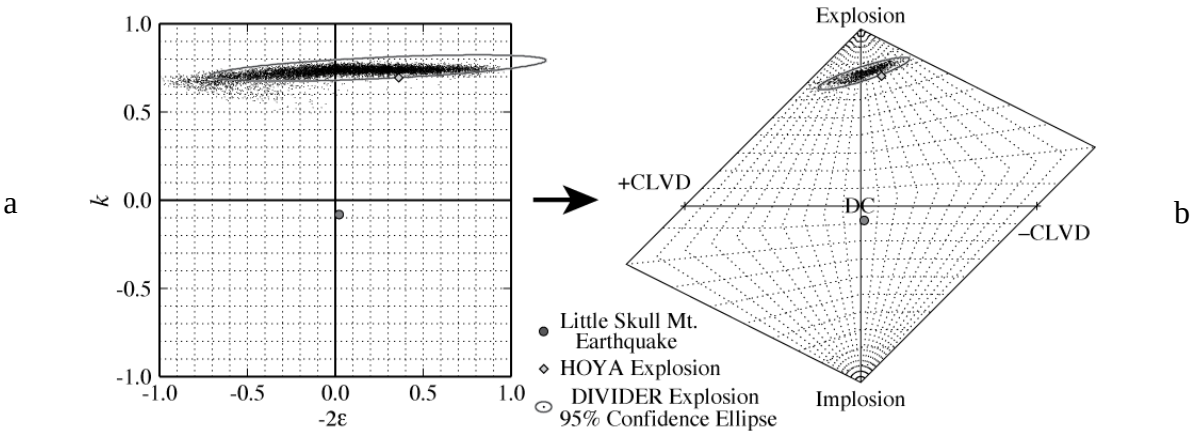

Figure 2. Source-type plot for the Little Skull Mt. earthquake (dark grey circle), NTS test HOYA (light grey diamond), and bootstrap population of the NTS test DIVIDER (black dots) along with its 95% confidence region (grey ellipse). a) The source-type parameters (k, -2ε) given on a linear plot. b) The source-type plot of Hudson et al. (1989) with theoretical mechanisms plotted as well.

defined by Bowers and Hudson (1999), where M_0 is equal to the sum of the isotropic moment (M_{ISO} = (M_{11}+M_{22}+M_{33})/3) and deviatoric moment (M_{DEV}), which is the largest deviatoric eigenvalue. For the Little Skull Mountain event we find $M_0 = 3.7 \times 10^{17}$ N-m (M_W = 5.6), and the solution has a negligible isotropic moment (M_{ISO} = -0.31×10^{17} N-m) so there is little change between the full and deviatoric solutions. The solution fits the data very well (Figure 2b) and is similar to the double-couple solution of Walter (1993), the deviatoric solution of Ichinose et al. (2003), and the full solution of Dreger and Woods (2002). With the same algorithm we calculate the full moment tensors of 17 nuclear test explosions at the Nevada Test Site (NTS) (Figure 1). In the case of explosions and collapses we calculate Green's functions at a depth of 1 km. The sensitivity of this assumption will be investigated later in the paper. An example of the analysis is given by the solution for the 1991 HOYA test, where the largest component in the decomposition is isotropic, and it contributes 70% of the total scalar moment.

Source-Type Plot

It is difficult to grasp the source-type from the standard focal mechanism plot for events with a large non-double-couple (DC) component. For example, one cannot discern the relative contributions of the isotropic and deviatoric components from the full focal mechanism for the HOYA explosion. In order to get at the tectonic contribution to the explosion, one could separate the deviatoric component into a DC and a compensated linear vector dipole (CLVD) that share the orientation of the major axis, but decompositions of this type are non-unique, where for example the DC and CLVD decomposition could be replaced by two DCs (see Julian et al. [1998]) for further decompositions). In an attempt to better characterize mechanisms, we follow the source-type analysis described in Hudson et al. (1989) and calculate -2ε and k, which are given by $\varepsilon = \frac{-m'_1}{|m'_3|}$ and $k = \frac{M_{ISO}}{|M_{ISO}| + |m'_3|}$, where m'_1, m'_2 and m'_3 are the deviatoric principal moments for the N, P, and T axes, respectively, and $|m'_1| \le |m'_2| \le |m'_3|$. A measure of the departure of the deviatoric component from a pure DC mechanism, ε, is 0 for a pure double-couple and ±0.5 for a pure CLVD. A measure of the volume change is k, where +1 would be a full explosion and −1 a full implosion. For the Little Skull Mountain earthquake and the NTS explosion, HOYA, -2ε and k are given in Figure 2a. The earthquake is almost at the origin, which defines a pure DC, whereas the nuclear test is near where a theoretical explosion would plot. In order to estimate formal error in the fit, we create moment tensor populations by bootstrapping the residuals of the fit $n$times with replacement and then use those populations of size n to calculate -2ε and k, resulting in their own populations to which we fit normal distributions. Figure 2a shows the population of n = 1,000 along with the 95% confidence region for the DIVIDER explosion. Increasing n resulted in no change to the confidence regions.

Hudson et al. (1989) transform the parameters -2ε and k so that the displayed plot will have equal normal probability areas based on the assumption that the smallest principal moments can take any value between ± the largest absolute principal moment (Julian et al., 1998). The plot derived this way is the source-type plot, and it is

shown in Figure 2b for the parameters from the Little Skull Mt. earthquake and HOYA explosion. Figure 2b also shows the transformed bootstrap population for the DIVIDER explosion and its associated 95% confidence region. The transformation makes the assumption of normality in the error distribution valid as can be seen by the improved fit of an error ellipse to the bootstrap population between Figure 2a and b. The Hudson et al. (1989) plot is a superior way to display source-type and analyze error in the parameters. The error ellipses are not shown for the Little Skull Mt. earthquake or HOYA explosion examples because the error regions are too small to notice a difference due to the transformation.

We carry out similar analyses for 11 more earthquakes and three collapses (one cavity and two mine) and produce the source-type plot in Figure 3 along with the 95% confidence regions. The nuclear tests occupy the region where $k > 0.5$, the earthquakes cluster near the origin, and the collapses plot almost exactly at (1,-5/9), which is the location for a closing crack in a Poisson solid. Deviations from these trends will be discussed later.

Sensitivity Analysis

The relatively small area of the confidence regions given in Figure 3 and the excellent synthetic seismogram fit to the data as quantified by VR gives us great confidence that the assumed velocity model and depth are correct and the estimated moment tensor solutions are robust. However, these measures of goodness-of-fit assume the underlying model used to invert the data is correct. In the following section we will test these assumptions with synthetic data from a theoretical explosion ($-2\varepsilon=0$, $k=1$) created for two experimental geometries. The first geometry, referred to as 'Ideal,' is eight stations at distance increments between 100 and 300 km each separated by 45°. The second station geometry mirrors the analysis for the HOYA explosion. The synthetic data are filtered in the same two bands (20–50s and 10–50s) used in the analysis and when combined with the two geometries results in 4 scenarios.

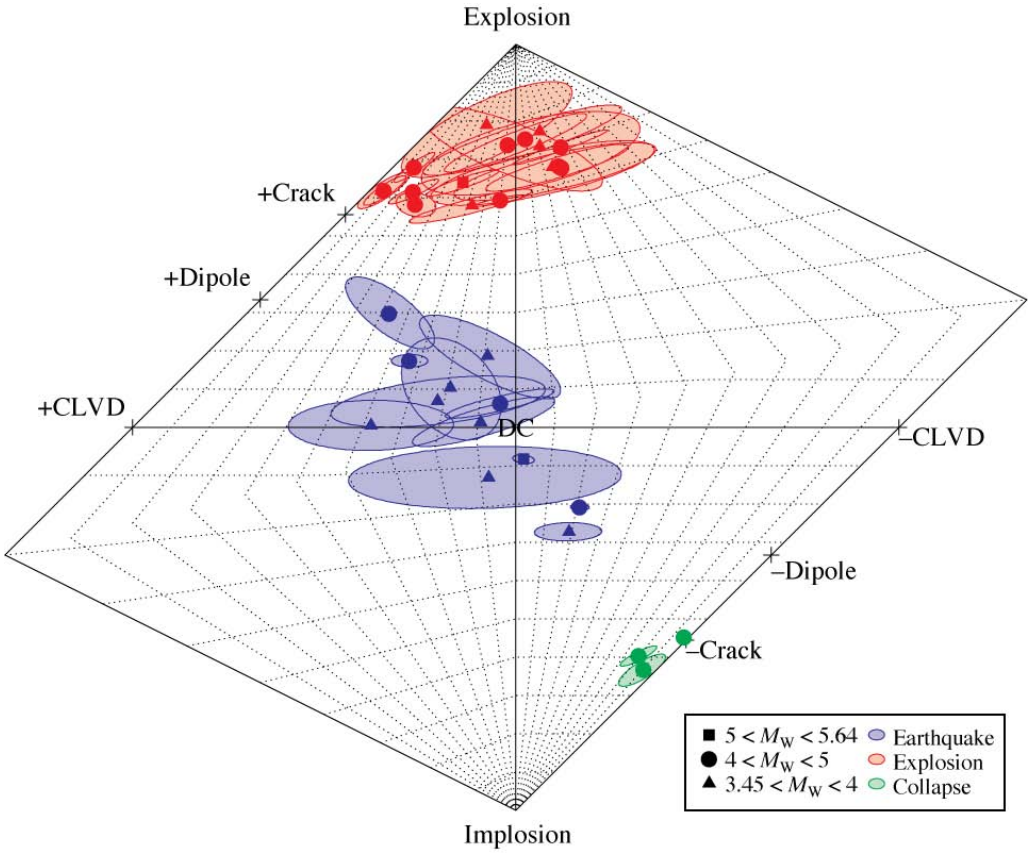

Figure 3. Source-type plot of the 12 earthquakes (blue), 17 explosions (red), 3 collapses (green), and their associated 95% confidence regions (shaded). The magnitude of the event is given by the symbol. The abscissa measures the amount of volume change for the source and the ordinate measures the departure from pure DC. Theoretical mechanisms (crosses) are plotted for comparison.

The error analysis presented above is due to a misfit of the data by the least-squares inversion. Part of the misfit may be due to nonstationary noise, and we test the sensitivity of the inversion to different SNRs. In order to best approximate real-world noise conditions, we derive the noise signal from data prior to the first arrival from the nuclear test METROPOLIS (10 March 1990) at station ANMO for all three components. The amplitude of this noise signal is bandpassed to match the synthetic data and multiplied by a factor so as to create a final synthetic signal with the desired SNR (ratio of synthetic data root-mean-square amplitude to noise root-mean-square amplitude).

The noise analysis has very little frequency dependence, so for clarity we only show results from the analysis in the 20–50 sec frequency band in Figure 4a. The Ideal configuration produces the best scenario where a large k is retrieved (>0.3) when the SNR is greater than 2. For all scenarios $k > 0.5$ when SNR > 5. Typically, we use data with an SNR greater than 10; however, there are a few cases where the SNR is close to 3. An example of this type of data is for the DIVIDER explosion, which produced a signal that was right on the limit of acceptable SNR but still produced a well-fit solution.

Another source of error not incorporated into the formal error analysis is incorrectly calculated Green's functions due to ignorance of the true event depth. The method that produces the results presented above attempts to find an optimal depth for the earthquakes by perturbing the reported depth a few kilometers, performing the inversion, and finding the best-fit solution. For all explosions and collapses, the depth is fixed at 1 km. If this method were to be used for an event with an unknown source type, the depth could be an important source of error, as well as an important parameter for identification. We perform another synthetic test in which an explosion at 1 km is inverted with Green's functions calculated at varying depths.

The source depth analysis is not greatly affected by the two station configurations considered here, therefore we only show results for the HOYA configuration in Figure 4b. The result at an incorrect depth of 2 km is virtually indistinguishable from the true answer. When the source is moved to 3 km depth there is a small step decrease in k due to a layer in the velocity model that begins at a 2.5-km depth. However, $k > 0.5$ for incorrect depths < 17 km with slightly more sensitivity in k and a worse fit in the high-frequency band (10–50 sec) compared to the low-frequency band (20–50 sec). The relative insensitivity of the solution to mislocated depth for an explosion is different than is observed for DC events. Dreger and Woods (2002) show that the VR of the Little Skull Mountain earthquake solution is definitively maximized at the assumed true event depth. Thus, while the depth sensitivity of explosions is poor, the method is able to determine the depth of non-explosion sources, which also provides an important level of event screening.

Finally, we test how error in the assumed Earth structure is mapped through the Green's functions to error in the solution. We start with the well-calibrated Song et al. (1996) velocity model (Table 1) and perturb the velocities and depths of the layers using averaged parameters from another plausible velocity model (WestUS; Ammon, 1999) and a model from Southern California (SoCal; Dreger and Helmberger, 1990).

In order to produce a sensitivity test that best mimics our analysis, we use the time shift rule to filter the models. This means that we only allow velocity models that produce Green's functions where the time shift between data and synthetics that produces the best-

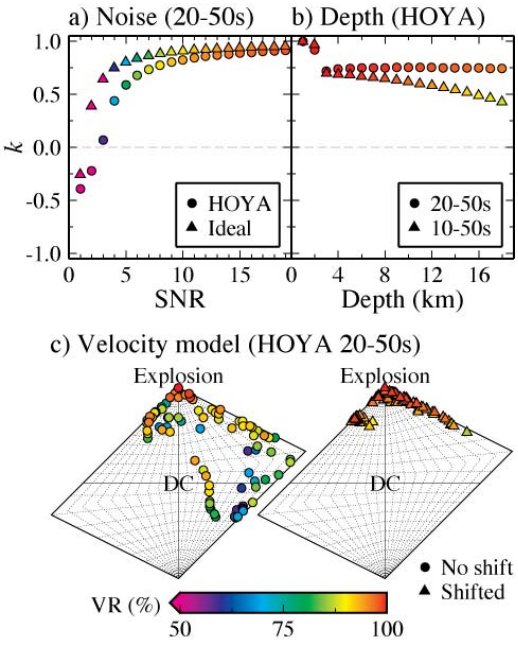

Figure 4. Sensitivity analysis. a) Noise is added to the inversion of 20-50 sec synthetic data while velocity model and depth (1 km) are kept fixed for the HOYA (circle) and Ideal (triangle) scenarios. b) The inversion using the HOYA configuration is carried out assuming an incorrect depth while the velocity model is kept fixed for data in the 20–50-sec (circle) and 10–50-sec (triangle) band. c) The inversion using the HOYA configuration for 20–50 sec synthetic data is carried out for different three-layer velocity models where the data are not shifted relative to the Green's functions (left panel, circles) and allowed to shift less than 5 sec (right panel, triangles). The symbols are colored as a function of VR.

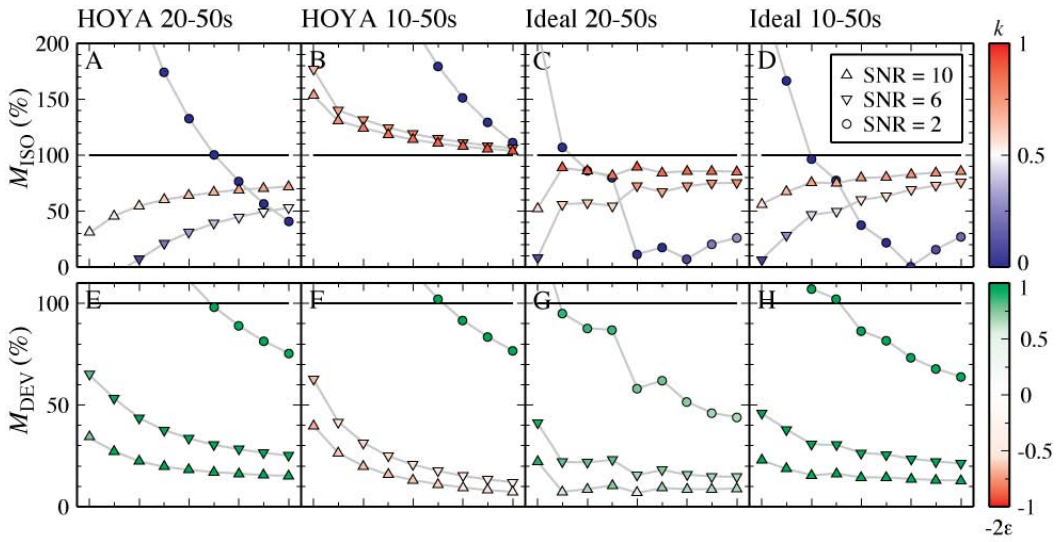

Figure 5. Vanishing traction sensitivity. Synthetic data for a pure explosion (k=1) is inverted at depths less than 1 km for varying SNR and the four scenarios discussed in the text. a-d) Resolved M_{ISO} for SNR values of 2 (circle) 6 (inverted triangle) and 10 (triangle) where the value for an inversion without noise (SNR=∞) is given by the black line (100%). k is given by the color. e-h) Resolved M_{DEV} for SNR values of 2, 6, and 10 with the same symbols, where the total scalar moment for an inversion without noise (SNR=∞) is given by the black line (100%), and M_{DEV} should be 0. -2ε is given by the color.

fit solution is less than or equal to 5 or 3 sec from the theoretical arrival time for high-pass corners of 0.05 or 0.10 Hz, respectively. Primarily due to the velocity model filtering there is little difference among the scenarios so we only show source-type plots for the HOYA configuration in the 20–50-sec frequency band in Figure 4c. For this scenario the number of acceptable models is reduced to 88, and although not all possible combinations of model parameters are used, each parameter perturbation given is employed at least once.

Without shifting, there are a few velocity models that produce well-fit solutions (VR>90%) with mechanisms that are almost purely DC. However, when shifting is allowed, all velocity models produce good fits with highly explosive sources (k~>0.4).

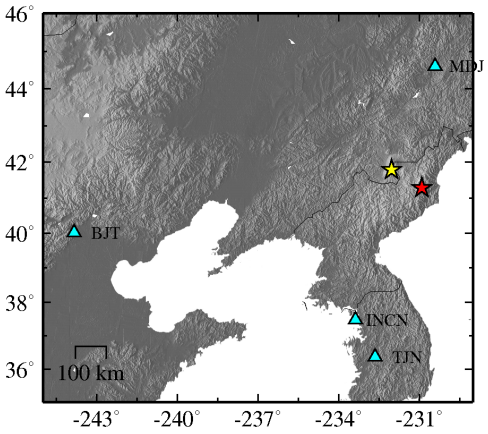

Figure 6. Map of the YSKP with the North Korea test (red star) and nearby earthquake (yellow star) as well as the stations used in this study (blue triangles).

Free-Surface Effects

Another consideration is the ability to resolve displacements for explosions near the surface. Since tractions normal to the vertical vanish at the free surface, the excitation coefficients associated with those tractions must vanish (Julian et al., 1998). Therefore, at the free surface the moments of M_{13}, M_{23}, and the isotropic part of the M_{ij} cannot be resolved. Given and Mellman (1986) showed that at a source depth of 1 km, the fundamental mode excitation functions associated with the moments listed previously effectively go to zero. We investigate the potential problems associated with vanishing traction at the free surface by inverting noisy data from a synthetic explosion source at depths between 200 and 1,000 m in a three-layer 1D velocity model using Green's functions calculated at those same depths.

The ability to resolve an explosive component is dependent on the station distribution, frequency, and SNR of the analysis, therefore Figure 5 shows all four scenarios. An explosive component (k>0.5) can be resolved under favorable noise conditions at a depth greater than 300 m for all scenarios, though with error in

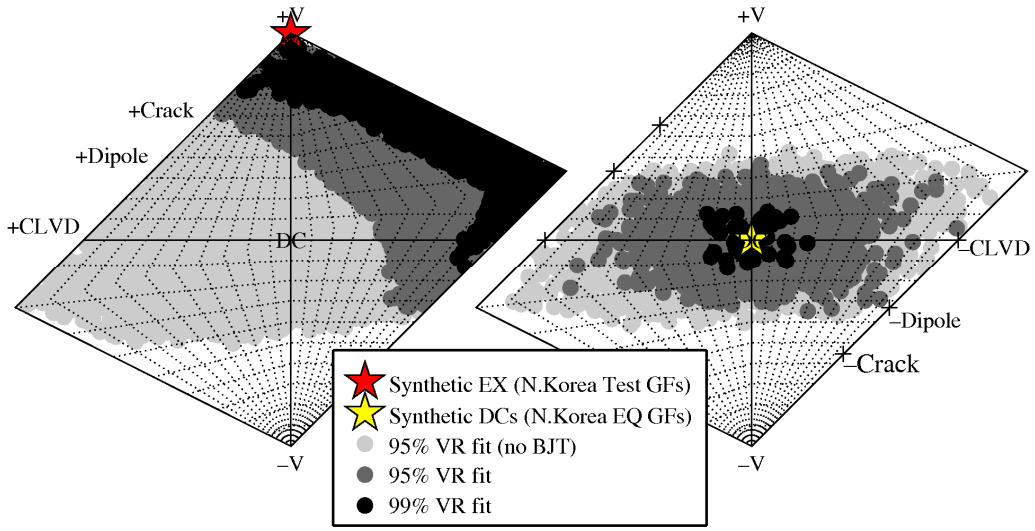

Figure 7. Network sensitivity solutions for the North Korea explosion (left) and earthquake (right). The actual solution is given by the stars and other solutions for a given threshold VR are shown. The 95% VR fit is given with (dark gray) and without station BJT (light gray).

M_{ISO} between 50–150% (Figure 5a-d). The error is inversely proportional to the depth. For all scenarios, but the HOYA configuration at 20–50 sec (Figure 5a), favorable noise means SNR ≥ 6. The change in M_{ISO} is due to a change in M_{33} relative to the other dipole components, and this produces an erroneous deviatoric component. The moment of deviatoric component can be up to 50% of the theoretical isotropic moment (Figure 5e-h) and since it is related to the error in M_{ISO} it is inversely proportional to the depth. At less than 200 m depth, the synthetic displacements become too small and the solution using these particular Green's functions is unreliable.

Network Sensitivity Solution

We extend the database of solutions by incorporating the North Korea test and a nearby earthquake that occurred on 16 December 2004 (Figure 6). We employ the records of four stations that recorded the events well in the period band of interest. We use the solutions to present a new way to estimate constraints on source-type. As discussed above, the ability to resolve a well-constrained solution is dependent on station configuration, data bandwidth, and SNR. The analysis presented in the previous section tried to assess error in those experimental conditions, but it is

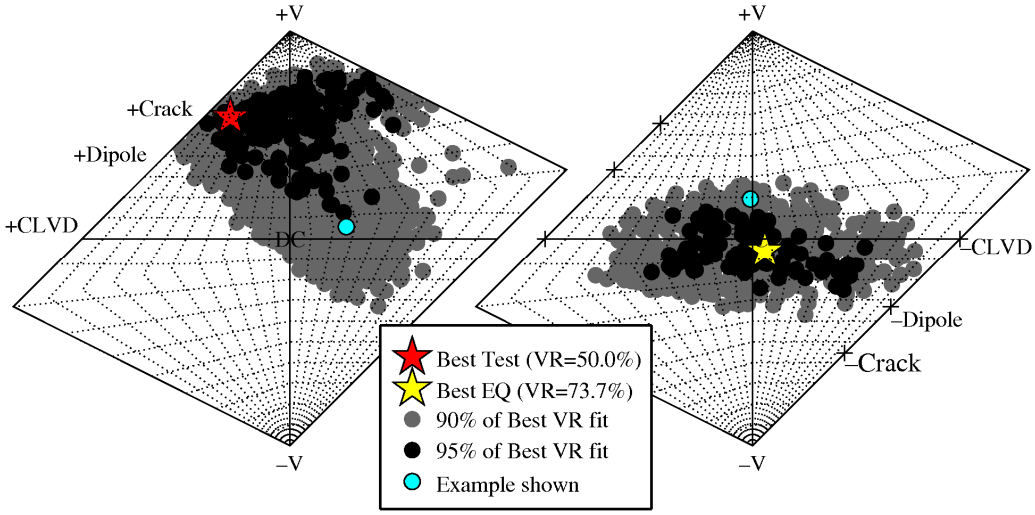

Figure 8. Network sensitivity solutions for the North Korea explosion station configuration and Green's functions (left) and earthquake setup (right). The best solution is given by the stars and different levels of fit, as quantified by VR, are shown. The source-types of the solutions given in Figures 10 and 11 are also shown (blue circles).

difficult to state steadfast rules for what source-types can be resolved for all conditions, when different conditions lead to different levels of confidence in the solution. Therefore, we calculate two types of forward confidence analyses, which we call network sensitivity solutions.

The first type of solution assumes a very large SNR and produces explosive or double-couple synthetics for a given station configuration using the Green's function employed in the inverse solution. In this case, the MDJ2 model is used to calculate the Green's functions. These model explosions and earthquakes are then compared with synthetic data produced by thousands of random seismic moment tensors that represent a uniform distribution of all possible moment tensors. A VR is calculated between the synthetics produced by the distribution of moment tensor and the perfect explosion or DC. In this way, we produce a source-type plot that shows solutions for a given threshold VR. Figure 7 shows the source-type plot constructed in this way for the North Korea test and nearby earthquake configurations. Without station BJT, most solutions fit the model explosive just as well as an explosion (Figure 7, left), whereas any source with an isotropic source greater than 50% does not fit the DC synthetics well (Figure 7, right). The use of this type of network sensitivity solution can give the user a feeling for what level of confidence can be expected in a given solution for the experimental setup employed.

The network sensitivity solution is also produced using the actual data in place of the synthetic explosion or DC. This plot can help the user understand the limits of confidence in the best solution. Figure 8 shows this type of network sensitivity solution for the same events as in Figure 7. The solutions are fairly well-constrained, but there

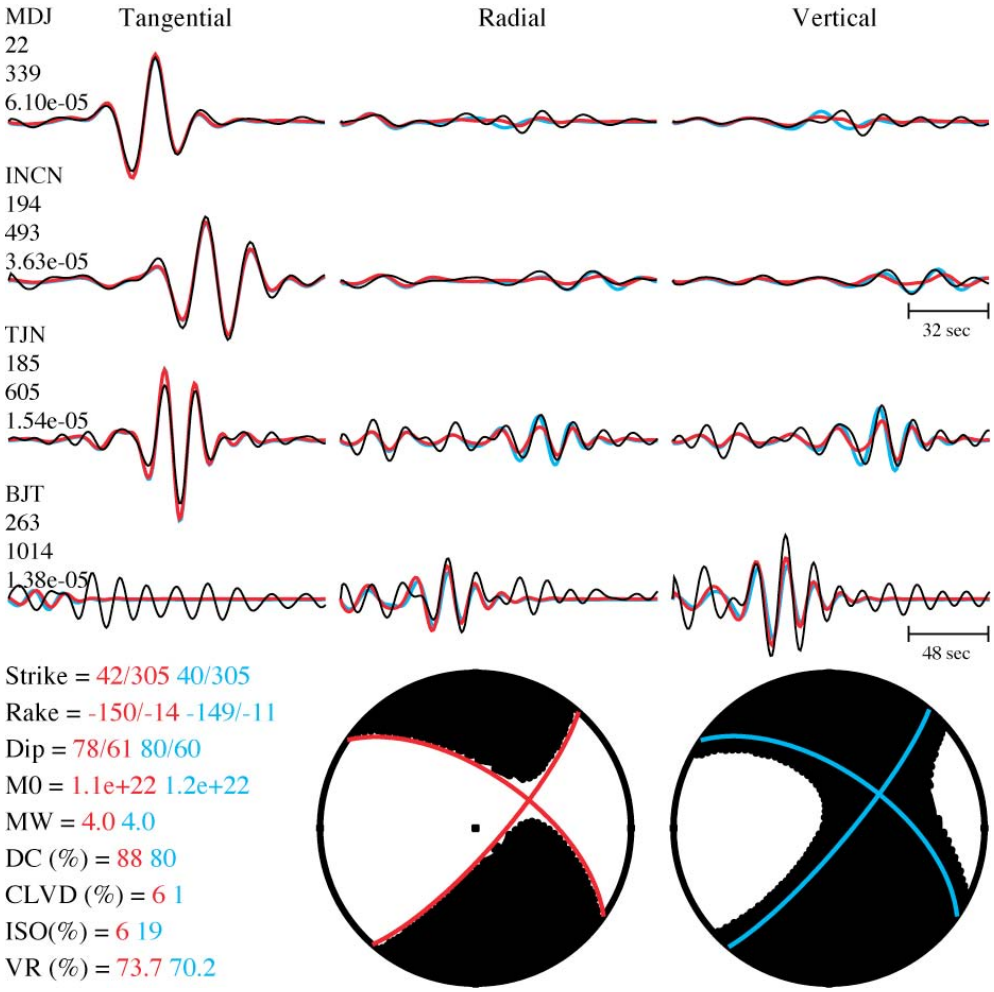

Figure 9. Waveform fits and focal mechanism for the best-fit (red) and fairly-well fit (blue) solutions using data from the earthquake near the North Korea test. The station name, azimuth, distance, and maximum displacement in cm are given next to the traces. Information on the sources is also given.

are some possible solutions with good VR that are near the DC section of the source-type plot, for the explosion data (Figure 8, left), and solutions that have some isotropic component, for the earthquake data (Figure 8, right). An understanding of what the VR means for these potentially confidence-busting solutions can be acquired by examining the data-fit. Figures 9 and 10 give the data fit for the best solutions (stars in Figure 8) and those for 'problematic' solutions with a high VR (blue circles in Figure 8). Visual inspection of the fits show that they are virtually indistinguishable and that both solutions may be possible given the data limitations. This is not so much a problem for the earthquake solution (Figure 9) since the percent DC is still relatively high, but the nuclear test solutions are fairly different (Figure 10).

CONCLUSIONS AND RECOMMENDATIONS

The populations of earthquakes, explosions, and collapses separate in the source-type plot. These initial results are very encouraging and suggest a discriminant that employs the source-type plot parameters $(-2\varepsilon, k)$. Another advantage of the source-type plot is its display of 2-D error regions. In this way one can test a hypothesis that an event has a non-DC component. The source-type analysis can also be utilized to estimate model-based error as well. The error introduced by ignorance of the event location and Earth structure can be calculated with a Monte Carlo approach, where several solutions are computed for a-priori distributions of the hypocentral location and Earth model obtained from independent analyses.

We try to give some insight to the depth sensitivity of the method with Figure 4b, which shows that the use of this

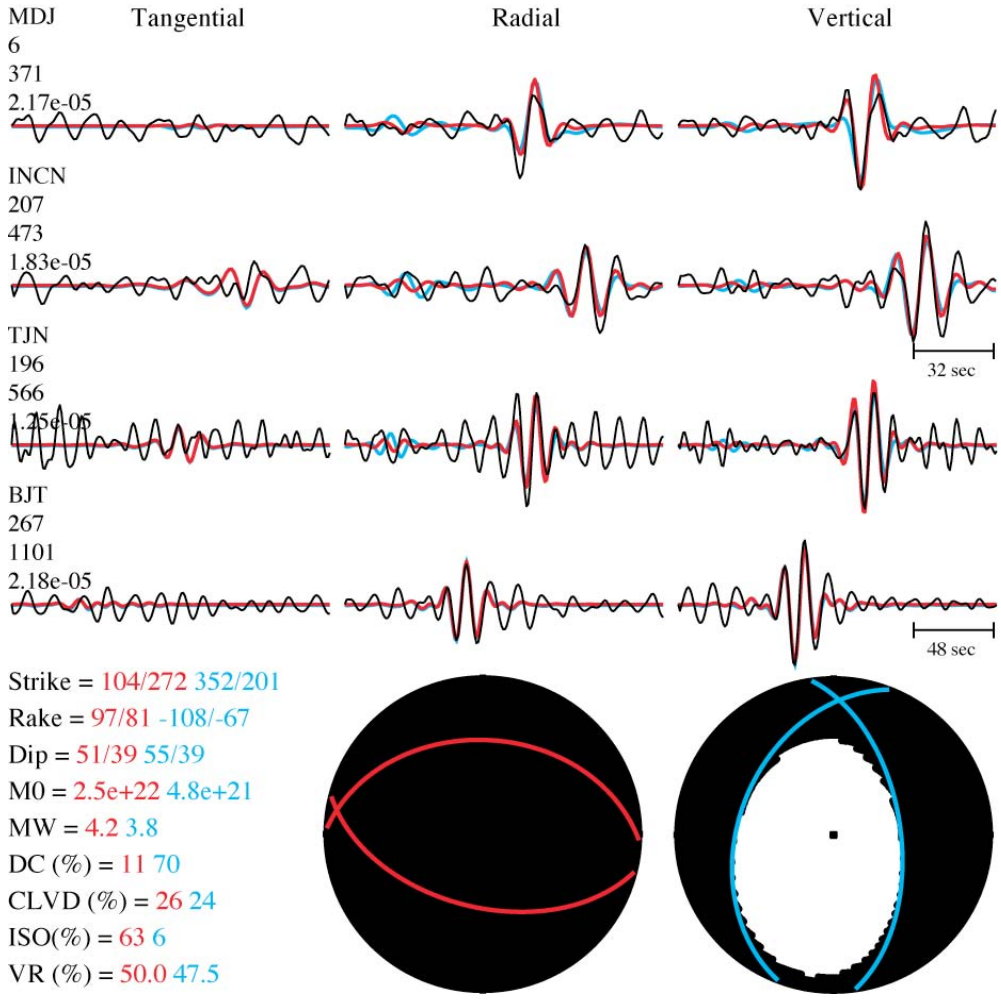

Figure 10. Waveform fits and focal mechanism for the best-fit (red) and fairly-well fit (blue) solutions using data from the North Korea test. See Figure 9 for more information.

method as a precise depth discriminant is not plausible for the frequencies used here, though sensitivity does increase for the higher-frequency band. These results are a demonstration of the fact that an isotropic radiation pattern has no sensitivity to takeoff angle, which depends on depth. As shown by Dreger and Woods (2002), there is limited resolution of the shallow depth of explosions using regional distance data. Although an explosive radiation pattern alone does not have depth sensitivity, the relative excitation of low-frequency body waves (Pnl) and Rayleigh waves does enable the method to discern the relatively shallower depths of explosions compared to earthquakes.

The velocity model analysis shown in Figure 4c suggests that the maximum-shift rule used in the analysis is a good proxy for evaluating the appropriateness of the velocity model. The level of departure of a given velocity model from the true model is station distribution, frequency, and SNR dependent. Therefore, it is a good idea to perform this style of sensitivity test to evaluate the amount of deviation a certain experimental setup will allow, because if the velocity model is poorly calibrated, then a good fit to the data can be obtained, but the solution may be inaccurate. The network sensitivity solution is a good way to accomplish this type of testing.

The change in moment due to the loss of traction at the free surface affects yield estimation, though event discrimination is still reliable at high SNR. A result of this change in moment is that the deviatoric moment becomes non-zero and could be significant at very shallow depths (Z<500 m) and low SNR (SNR<6). The moment manifests as a CLVD component, which means that interpretation of non-isotropic energy may be flawed for shallow events even with high SNR data. Though, as Figure 5 suggests, this effect is station configuration, frequency, and SNR dependent.

ACKNOWLEDGEMENTS

We thank Jeff Stevens for discussions regarding free surface effects and Howard Patton for insights on the CLVD contribution to the explosion source. We also thank Bruce Julian for scripts to make the source-type plots.

REFERENCES

Bowers, D. and J. A. Hudson (1999). Defining the scalar moment of a seismic source with a general moment tensor, *Bull. Seis. Soc. Am.* 89: (5), 1390–1394.

Dreger, D. and B. Woods (2002). Regional distance seismic moment tensors of nuclear explosions; seismic source mechanism through moment tensors, *Tectonophysics* 356: (1–3), 139–156.

Given, J. W. and G. R. Mellman (1986). Estimating explosion and tectonic release source parameters of underground nuclear explosions from Rayleigh and Love wave observations, Tech. rep., Sierra Geophysics Report No. SGI-R-86-126, Kirkland, WA.

Herrmann, R. B. and K. Hutchensen (1993). Quantification of MLg for small explosion, Tech. rep., Phillips Laboratory Report PL-TR-93-2070.

Hudson, J. A., R. G. Pearce, R. G., and R. M. Rogers (1989). Source type plot for inversion of the moment tensor, *J. Geophys. Res*. 9: (B1), 765–774.

Ichinose, G. A., J. G. Anderson, K. D. Smith and Y. Zeng (2003). Source parameters of Eastern California and Western Nevada earthquakes from regional moment tensor inversion, *Bull. Seis. Soc. Am*. 93: (1), 61–84.

Julian, B. R., A. D. Miller, and G. R. Foulger (1998). Non-double-couple earthquakes; 1. Theory, *Rev. Geophys* 36: (4), 525–549.

Langston, C. A. (1981). Source inversion of seismic waveforms; the Koyna, India, earthquakes of 13 September 1967, *Bull. Seis. Soc. Am*. 71: (1), 1–24.

Minson, S. and D. Dreger (2008). Improved seismic moment tensor inversion, *Geophys J. Int.*

Saikia, C. K. (1994). Modified frequency-wavenumber algorithm for regional seismograms using Filon's quadrature; modelling of Lg waves in Eastern North America, *Geophys. J. Int*. 118: (1), 142–158.

Song, X. J., D. V. Helmberger and L. Zhao (1996). Broad-band modelling of regional seismograms; the basin and range crustal structure, *Geophys. J. Int*. 125: (1), 15–29.

Walter, W. R. (1993). Source parameters of the June 29, 1992 Little Skull Mountain earthquake from complete regional waveforms at a single station, *Geophys. Res. Lett*. 20: (5), 403–406.

Walter, W. R., K. D. Smith, J. L. O'Boyle, T. F. Hauk, F. Ryall, S. D. Ruppert, S. C. Myers, R. Abbot, and D. A. Dodge (2004). An assembled western United States Dataset for regional seismic analysis, LLNL, UCRL-TR-206630.